Chinese Chemical Letters 34 (2023) 107576

Contents lists available at ScienceDirect

Chinese Chemical Letters

journal homepage: www.elsevier.com/locate/cclet

# BODIPY-based supramolecular fluorescent metallacages

Yute Wang, Yi Qin*, Xiaoli Zhao, Peipei Jia*, Zhiyong Zeng, Lin Xu*

*Shanghai Key Laboratory of Green Chemistry and Chemical Processes, Shanghai Frontiers Science Center of Molecule Intelligent Syntheses, School of Chemistry and Molecular Engineering, East China Normal University, Shanghai 200062, China*

ARTICLE INFO

*Article history:*
Received 14 March 2022
Revised 29 May 2022
Accepted 31 May 2022
Available online 3 June 2022

*Keywords:*
Metallacage
BODIPY
Coordination-driven self-assembly
Tetrahedron
Fluorescence

ABSTRACT

During the past few years, the construction of BODIPY-based supramolecular fluorescent metallacages through coordination-driven self-assembly has gained increasing interest due to their unique photophysical properties and applications in catalysis, sensing, and bioimaging. In consideration of the rapid development of this field, it is time to summarize recent developments involving BODIPY-based metallacages. In this review, a comprehensive summary of the construction of BODIPY-based metallacages as well as their photophysical properties and applications will be presented.



## 1. Introduction

Coordination-driven self-assembly has proven to be a powerful synthetic methodology for the construction of discrete supramolecular coordination complexes (SCCs) with well-defined shapes and sizes [1–12]. Due to the diverse structural motifs including metals and ligands, that are accessible *via* coordination chemistry, a variety of SCCs with delicate and elegant structures, including two-dimensional (2D) metallacycles and three-dimensional (3D) metallacages, have been successfully constructed during the past few decades [13–26]. Compared to the 2D metallacycles and metal-organic frameworks (MOFs) [27], metallacages inherently showed discrete 3D structures with enclosed cavities. The good solubility as well as the cavities of the metallacages endow them with ability to encapsulate diverse guests, thus offering a privileged platform for molecular sensing, catalysis, drug delivery, *etc.* [28–37]. Furthermore, supramolecular cages decorated with fluorescent chromophores have displayed distinctive photophysical properties and thus could be further applied in photocatalysis, light harvesting, sensing and biological applications, which have promoted the development of supramolecular chemistry and materials science [38–48].

As classic fluorescent chromophores, BODIPYs ($BF_2$-chelated dipyrromethenes) exhibit outstanding features, such as large molar absorption coefficients, high emission fluorescence quantum yields, efficient singlet oxygen generation, and excellent chemical stability [49–53]. Moreover, the relatively planar and linear conformation and easy functionalization make BODIPYs ideal candidate ligands for supramolecular self-assembly. In the past few decades, a growing number of supramolecular self-assembled systems based on BODIPYs have been constructed, and they have displayed widespread applications in light harvesting, fluorescent sensors, photodynamic therapy (PDT), *etc.* [54–60]. In 2020, we reviewed the syntheses, properties and applications of BODIPY-based macrocycles [61]. Compared to 2D BODIPY-based macrocycles, 3D BODIPY-based metallacages showed some unique photophysical properties and functions, such as (1) the inherent cavities of BODIPY-based metallacages make them good platforms for investigating excited state energy transfer between hosts and guests; (2) the relatively planar structure of BODIPY enables additional $\pi$-$\pi$ interactions with other building blocks, which is beneficial for the formation of more complexes and sophisticated supramolecular architectures; and (3) integrating BODIPY subunits and other fluorescent chromophores into one entity may lead to white light emission from a single compound. In the past few years, a series of BODIPY-based cages have been prepared, and their properties and applications have been studied in detail. The structure of BODIPY is shown in Scheme 1, and BODIPY was generally adopted as a bidentate linear ligand (with modifications at the $\beta$ positions), which was beneficial for preparation of tetrahedral cages through subcomponent self-assembly [62]. On the other hand, BODIPY subunits could also be attached to the peripheries of cages. For example, the meso position of BODIPY could be modified with pyridines, which were then coordinated with metals such as Pd and Pt to construct $M_nL_{2n}$-type cages. Notably, the shapes and sizes of the BODIPY-based cages have an important influence on their host-guest chem-

* Corresponding authors.
*E-mail addresses:* qinyihuaxue@126.com (Y. Qin), 51174300063@stu.ecnu.edu.cn (P. Jia), lxu@chem.ecnu.edu.cn (L. Xu).

https://doi.org/10.1016/j.cclet.2022.05.090
1001-8417/

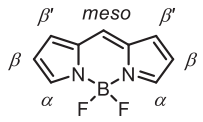


**Scheme 1.** Chemical structure of BODIPY.

istry and photophysical properties. In this review, we will focus on the preparation, photophysical and photochemical properties and applications of BODIPY-based cages.

## 2. BODIPY-based metallacages

### *2.1. BODIPY-based metallacages via Fe or Zn coordination*

In consideration of the octahedral coordination mode of transition metals such as Fe and Zn, the self-assembly of the linear BODIPY-based ligand with these metals always led to the formation of tetrahedral cages through subcomponent self-assembly. The BODIPY-based ligands were prepared from the modification of BODIPY fluorophores with amino groups or 2-formaldehyde pyridines at the $\beta$ positions and the subsequent self-assembly of the BODIPY-based ligands with other subcomponents and metal ions led to formation of metallacages with high yields. The fluorescence of the metallacages were red-shifted compared to the classic BODIPY fluorophore and the photosensitization property of the metallacages was alternative. In addition, the multi-fluorophore interactions also played an important role in the photophysical/chemical properties of the metallacages.

In 2014, Nitschke and co-workers reported the first BODIPY-based tetrahedral cages and investigated their photophysical properties [63]. Treatment of BODIPY-functionalized diamine ligand **1** with **2** or **3** and metal ions ($Fe^{2+}$ and $Zn^{2+}$) afforded tetrahedral cage **4**, **5**, and **6** (Fig. 1a), respectively. The cages were well characterized with NMR and mass spectrometry. It should be noted that the NMR spectra of **4-6** were complex due to the presence of stereoisomers. Molecular simulations indicated that **4-6** adopted a classic tetrahedral conformation [64] and that the mesityl groups of BODIPY were randomly pointed in any direction (into the cavities or out of the cavities), which increased the structural complexity of the cages (Fig. 1b). In addition, the formation of cages showed a great influence on absorption and emission by the chromophore. Compared to BODIPY-containing ligand **1**, all cages **4**-**6** exhibited blue-shifted absorptions (approximately 70–100 nm) and recovered fluorescence with fluorescence quantum yields of 0.012, 0.015 and 0.055, respectively. Moreover, the emission of the pyrene subunit of **5** was quenched upon cage formation. Furthermore, the host-guest properties of **4**-**6** were studied with anionic guests. The combined results from spectrographic data and NMR data revealed that cages **4**-**6** exhibited strong binding affinity with acetate and azide and moderate binding affinity with fluoride and chloride, whereas they did not respond to bromide, iodide, nitrate, hexafluorophosphate, triflate, perchlorate or tetrafluoroborate. Upon addition of acetate into a solution of cage **4**, the absorption maximum was changed from 555 nm to 606 nm (Fig. 1c), and this accompanied by generation of four isosbestic points at 588, 464, 268 and 252 nm. The fluorescence intensity of **4** at 653 nm also showed a 25-fold increase (Fig. 1d). Thus, by taking advantage of this dual-mode recognition, a test-paper strip test was designed. It showed good response to certain anions, and it could be used for anion detection in aqueous media (Fig. 1e). Further experiments indicated that anion recognition was probably due to partial disassembly of cages, and the electrostatic and anion-$\pi$ interactions between the host and guests also made a great difference. In addition, the cages showed low binding affinity with polycyclic aromatic hydrocarbons (PAHs), such as perylene, naphthalene, and anthracene (Fig. 1f). Considering the multichromophoric character of the host-guest complex (perylene, pyrene and BODIPY as blue, green and red emitters, respectively), white light emission was realized with a fluorescence quantum yield of 0.11 and CIE coordinates of (0.30, 0.36) by fine-tuning the proportion of the guest perylene (Fig. 1g). Moreover, the cages could also be employed as reaction-based sensors for amino acid recognition. The addition of amino acids such as cysteine led to changes in the absorption band as well as the quenching of BODIPY fluorescence, which resulted from amine exchange between the amino acid and the BODIPY-containing ligand (Fig. 1h). The proposed mechanism is that a transient complex [**4**.amino acid] with more brilliant fluorescence was formed upon the addition of amino acid initially and the subsequent formation of the amino-acid-based mononuclear complexes with almost no fluorescence due to ligand exchange (Fig. 1i). In conclusion, a series of BODIPY-based tetrahedral cages with multiple functionalities were prepared in this work, which laid the foundation for construction of fluorescent SCCs for various applications.

Since BODIPY is a good photosensitizer with excellent capacity for singlet oxygen ($^1O_2$) generation, Nitschke *et al.* reported the synthesis of a series of BODIPY-based tetrahedral cages and studied their autocatalytic character through photooxidation-driven ligand exchange [65]. BODIPY-containing cages **13**-**17** were readily obtained from the reaction of bis(formylpyridyl)-functionalized BODIPY-containing ligand **7** with various diamines **8**-**12** in $CH_3CN$ (Fig. 2a). After the cages were well characterized with NMR and mass spectrometry, their $^1O_2$ generation ability was investigated with the $^1O_2$ indicator 1,3-diphenylisobenzofuran (DPBF) (Fig. 2b). The quantum yields of singlet oxygen generation of **13**-**15** and **17** are 0.01-0.02 and 0.045, respectively. The relatively high $^1O_2$ generation capability of 17 was ascribed to enhanced intersystem crossing (ISC) resulting from the presence of the heavy atom iodine. Moreover, the methylthio groups of cage **15** were oxidized to sulfoxides by $^1O_2$ to produce cage **16**. In addition, due to the dynamic nature of subcomponent self-assembly, amine exchange occurred through addition of extra diamine, and previous studies revealed that it was easier for electron-rich ligands to displace electron-deficient ligands [66]. Moreover, the Hammett parameters of **8**-**12** were 0.50, -0.27, 0.0, 0.49 and 0.18, respectively (the more electron-poor aniline showed the larger Hammett parameters) [67]. Therefore, addition of amine ligand **12** into cage **15** led to the rapid release of amine **10** initially due to ligand exchange (Fig. 2c), which was calculated from integration of the NMR spectrum. Then, the release rate gradually declined because equilibrium was reached. However, after an induction period, a large increase in the proportion of **10** released was observed, which was ascribed to ligand exchange between **12** and photooxidation-generated amine ligand **11**. Owing to the more electron-deficient character of sulfoxides **11**, the incorporation of ligand **12** into the cage occurred more rapidly as the photoreaction proceeded, subsequently resulting in enhanced $^1O_2$ generation. Thus, an autocatalytic system based on photooxidation-driven ligand exchange was successfully constructed (Fig. 2d). A control experiment was also conducted, and the results revealed that no second exponential rise was observed in the absence of $O_2$ and light. Subsequent exposure to $O_2$ and light also led to a rapid increase in the rate for release of **10**, further confirming its autocatalytic character. This research successfully realized the construction of an autocatalytic system based on photooxidation-driven ligand exchange within BODIPY-based tetrahedral cages, which is of great significance for designing artificial supramolecular systems to understand the complexity of nature.

Investigations of excited-state photophysics have played an important role in designing optical materials for artificial photosynthesis and solar energy conversion. In 2017, Nitschke and coworkers synthesized a series of homoleptic and heteroleptic BODIPY-

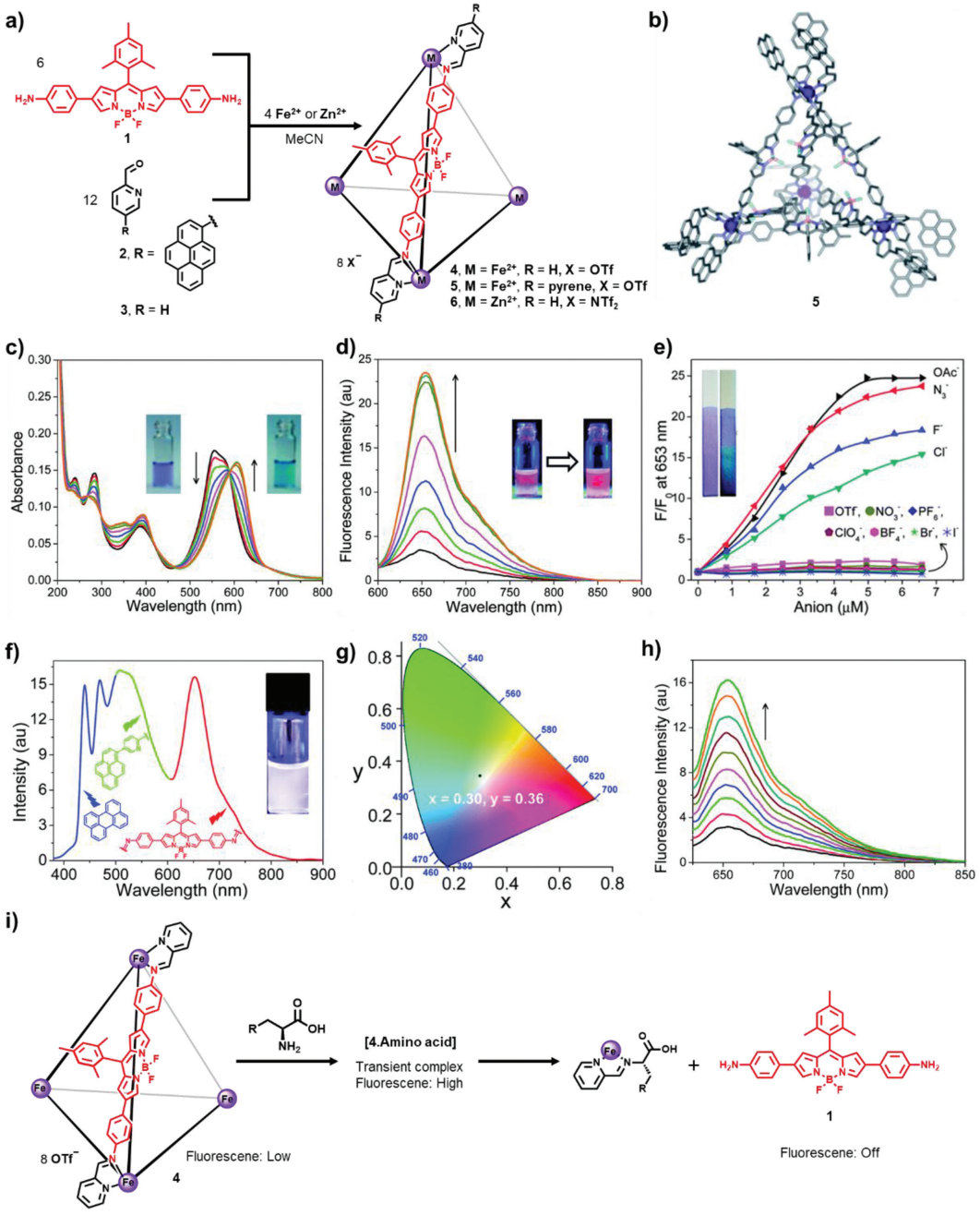


**Fig. 1.** (a) Synthesis of BODIPY-containing cages **4**-**6**. (b) Energy minimized structure of cage **5**. (c) Absorption spectral changes for cage **4** upon addition of tetrabutylammonium acetate in acetonitrile. (d) Fluorescence spectral changes for cage **4** upon addition of tetrabutylammonium acetate in acetonitrile. (e) Relative changes in the fluorescence intensity of **4** at 653 nm in the presence of selected anions (the inset shows photographs of a filter paper test strip). (f) Fluorescence spectrum and photograph of a mixture of **5** and perylene in a suitable ratio in acetonitrile. (g) CIE coordinates for the white-light emission from a mixture of **5** and perylene in a suitable ratio in acetonitrile. (h) Fluorescence spectral changes for cage **4** upon addition of cysteine in 50% acetonitrile/water mixture. (i) Proposed mechanism of amino acid recognition by **4**. Reproduced with permission [63]. Copyright 2014, Royal Society of Chemistry.

containing cages and studied their excited-state photophysics in depth [68]. The homoleptic BODIPY-containing cages **23** and **24** were readily obtained by a similar method to cage **4**. Heteroleptic cages **25** and **26** were prepared through a reaction of diamine **21**, diamine **22**, 2-formylpyridine and the metal ion ($Fe^{2+}$ or $Zn^{2+}$) in a 3:3:12:4 ratio (Fig. 3a), and NMR and ESI-MS results showed that all seven possible cages were distributed statistically in the mixture. Due to partial disassembly of the cages at low concentrations, the ligands and cages were embedded in a polymer matrix (polymethyl methacrylate, PMMA) to form films for further photophysical studies. The absorption spectra for cages **23** and **24** exhibited narrow and blue-shifted absorption peaks compared to their diamine ligands **21** and **22** (Fig. 3b), respectively, due to suppression of charge-transfer character upon cage formation. In particular, the absorption spectrum of **23** showed a long wavelength tail, probably due to formation of "dim" coupled states with head-to-tail couple interactions, and the higher-energy peak corresponded to "bright" couple states with maximum numbers of head-to-head couple interactions. For cage **24**, variation between the "bright" and "dim" states was not distinct due to the disturbed-transition dipole moments resulting from the presence of bulky TIPS groups. In addition, cages **23** and **24** showed almost no emis-

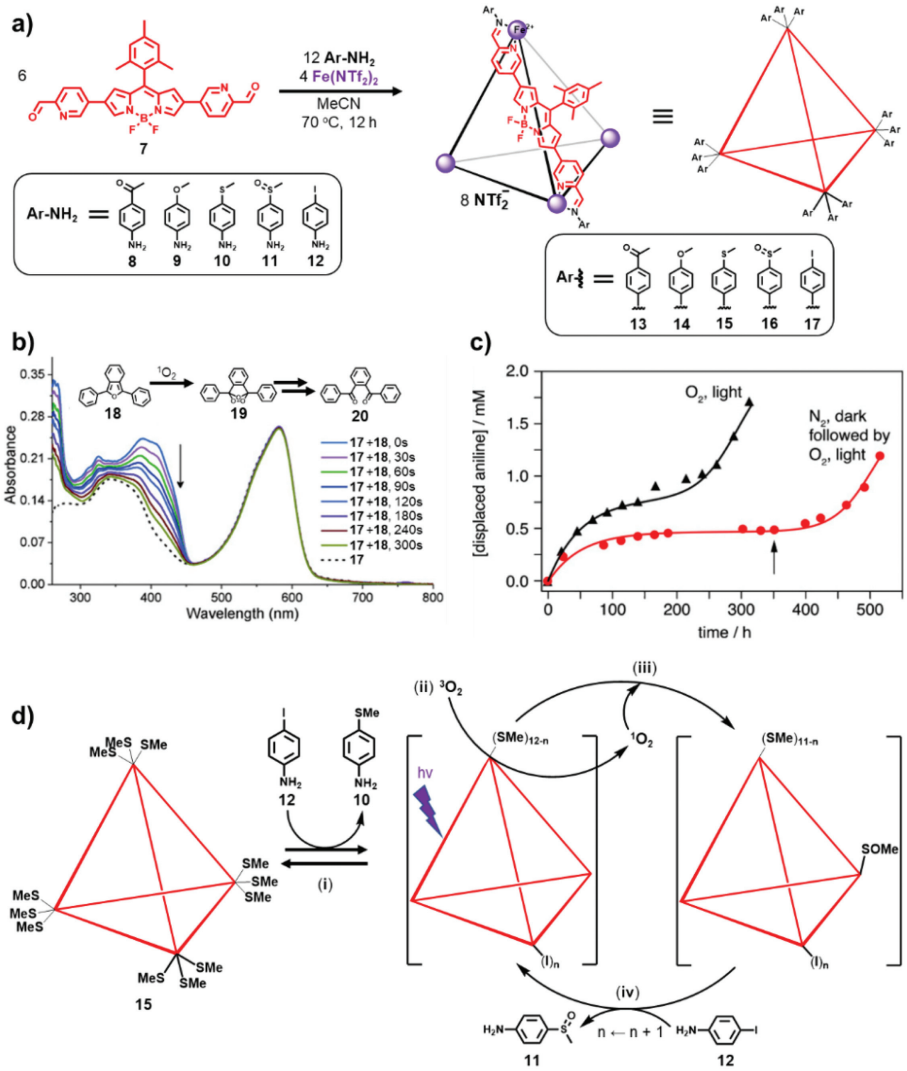


**Fig. 2.** (a) Syntheses of BODIPY-containing cages **13**-**17** from precursors **8**-**12**. (b) $^1O_2$ measurement with cage **17** by using the indicator DPBF. (c) The concentration of the displaced **10** under different reaction conditions. (d) Schematic representation of the autocatalytic photooxidation process of cage **15** after addition of ligand **12**: (i) Equilibrium subcomponent substitution occurred to a limited degree in the dark; (ii) as the reaction continued, more ligands **12** were incorporated into the cages, resulting in more efficient $^1O_2$ generation from $^3O_2$; (iii) $^1O_2$ oxidized **10** in cage **15** to electron-poor **11** residues, which were then (iv) displaced by **12**, increasing by one the number (n) of **12** residues. Reproduced with permission [65]. Copyright 2015, Wiley Publishing Group.

sion (QY < $10^{-4}$), which differed from the typical BODIPY chromophore. Transient grating photoluminescence spectroscopy measurements indicated that the fluorescence quenching of the cages was probably attributable to excited-state interchromophore coupling, leading to formation of dark states from bright states. Furthermore, transient absorption (TA) spectroscopy was performed to investigate their photophysics, and the results indicated that the excited states could be classified into three species (Figs. 3c–f). Species I was present from the initial state through a 250 fs lifetime and was indicated primarily by a ground-state bleaching (GSB) peak. Subsequent fast conversion from species I to species II was probably due to conformational flexibility of the cage framework, which led to the dramatic decrease in the peak at 515 nm. Species III, which was derived from the change in the balance of GSB and first-derivative features, showed the longest lifetime, and the conversion from species II to species III was inferred to come from structural changes in the cage geometry. The combined results from transient grating photoluminescence spectroscopy and transient absorption (TA) spectroscopy indicated that dipole frustration of the bright state was dominant and a nonemissive state was subsequently formed (Fig. 3g), which was consistent with the results from the absorption and fluorescence spectra. For the heteroleptic cages **25** and **26**, TA spectroscopy was not consistent with a simple combination of cage **23** and cage **24**, suggesting that strong chromophore coupling existed in the ground state. In addition, the effect of chromophore coupling was slightly weaker for **26** than for **25**, revealing that partial through-bond interactions also participated in excitation energy delocalization. It should be noted that the BODIPY-based cages exhibited distinctive chromophore coupling, which differed substantially from the perylene-based cages reported by Frischmann *et al.* [69,70], and the small size (3 nm) of the cages played the most important role. Furthermore, the host-guest properties of the cages were investigated, and the results indicated that the cages could bind $C_{60}$ or $C_{70}$ with negligible changes in their absorption spectra. TA spectroscopy for the host-guest complexes was significantly different from that of the empty cages (Fig. 4). For example, photoinduced absorption (PIA) beyond 650 nm was observed over hundreds of picoseconds for the host-guest complex, probably due to charge transfer between the cage and $C_{60}$ or $C_{70}$, and the charge transfer process

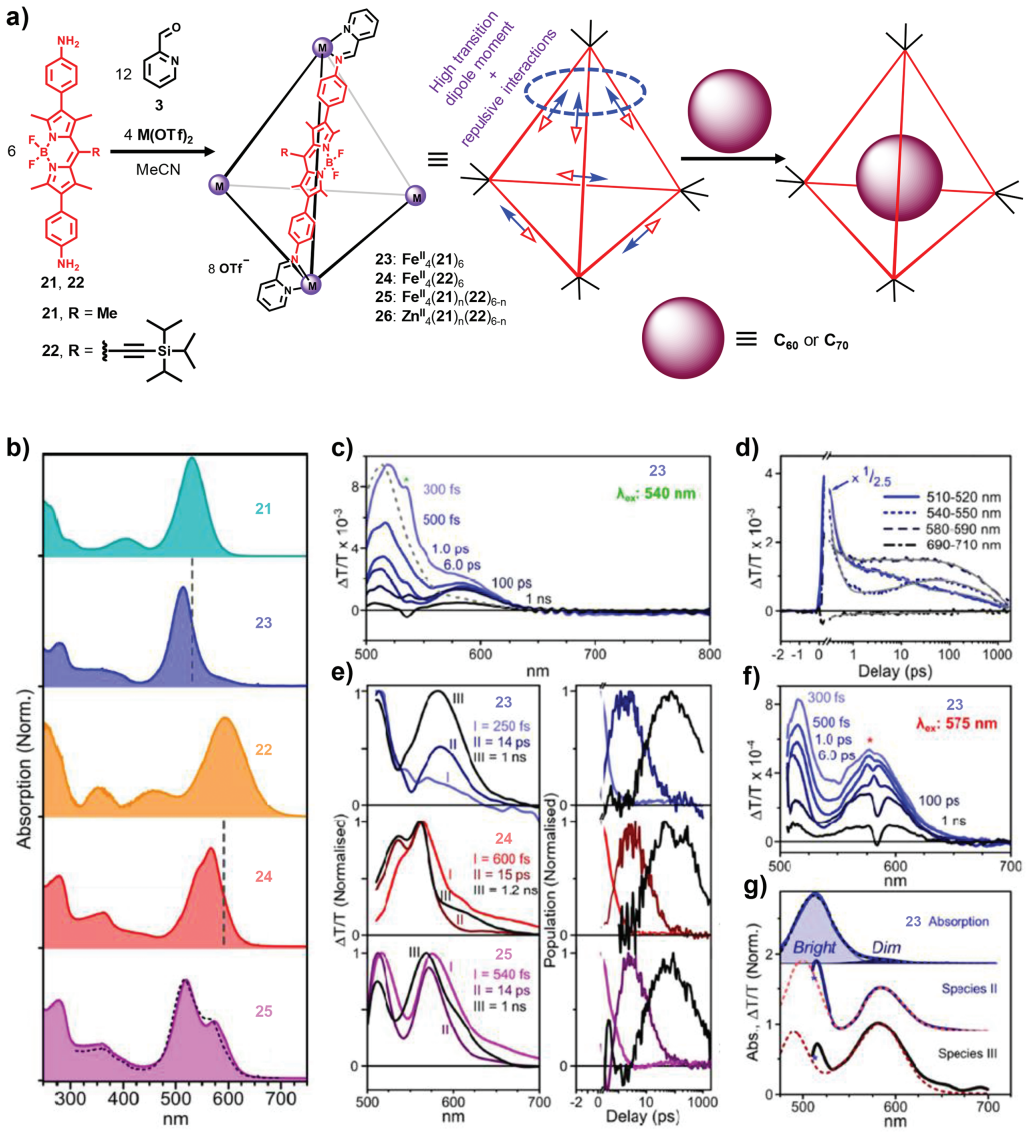


**Fig. 3.** (a) Synthesis of BODIPY-containing cages **23**-**26** and host-guest binding with fullerenes. (b) Absorption spectra of ligands **21**-**22** and cages **23**-**25**. (c) Transient absorption spectra of empty cage **23** upon excitation at 540 nm. (d) Corresponding decay kinetics for cage **23** averaged over the indicated spectral regions. (e) Decomposition into time-independent species-associated spectra (left) and population kinetics (right) reveals smooth, sequential conversion. (f) Transient absorption spectra of cage **23** upon excitation at 575 nm, indicating the absence of species I. (g) Absorption spectrum of cage **23** (top, solid) and subsequent decomposition into bright and dim aggregate contributions (dashed). Reproduced with permission [68]. Copyright 2017, American Chemical Society.

depended largely on the pump wavelength. In conclusion, BODIPY-based cages exhibiting excitation energy localization and transfer to guests were successfully constructed, and this will provide guidance for the design of fluorescent supramolecular systems for optical applications.

### 2.2. BODIPY-based metallacages via Pt or Pd coordination

As for the planar coordination mode of Pt and Pd as well as the development maturity of Pt or Pd-based SCCs, the $M_nL_{2n}$-type BODIPY-based cages was readily obtained *via* Pt or Pd coordination. The BODIPY-based ligands were prepared from the modification of BODIPY fluorophores with pyridines at the $\beta$ positions or the meso position. Then the ligands were self-assembled with Pt or Pd metals, affording the BODIPY-based metallacages with structural complexity. In addition, owing to that the BODIPY fluorophores were usually attached to the peripheries of cages, the photophysical/chemical properties of the metallacages were generally similar to the ligands.

In comparison to monocomponent supramolecular cages, multicomponent emissive cages can combine different fluorescent chromophores into one system, which often exhibit unique properties and functions. In 2017, Zhang *et al.* reported the syntheses of multicomponent emissive Pt(II) cages based on the chromophores of BODIPY and tetraphenylethene (TPE) [71]. Addition of the TPE-functionalized carboxylate ligand **27**, 90° Pt(II) acceptors **31** and dipyridyl ligands **28**–**30** in a 1:4:2 ratio in acetone/$H_2O$ provided cages **32**–**34**, respectively (Fig. 5a), with yields of more than 90%. All cages were well characterized by NMR spectroscopy, ESI-TOF-MS, UV–visible and fluorescence spectroscopy. The results from molecular stimulations revealed that the cages adopted tetragonal prismatic conformations and the TPE subunits, dipyridyl ligands and 90° Pt(II) acceptors were employed as the faces, pillars, and corners, respectively (Figs. 5b–d). Further spectroscopic experiments indicated that **32** and **33** exhibited main absorption

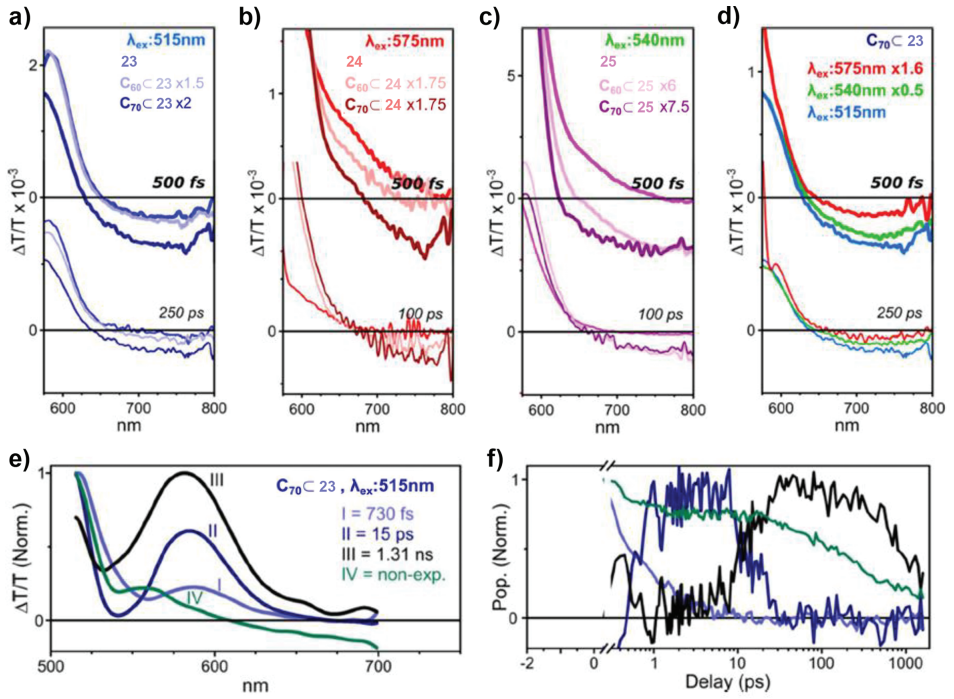


**Fig. 4.** Transient absorption spectra of (a) **23**, **C60⊂23**, and **C70⊂23** upon excitation at 515 nm; (b) **24**, **C60⊂24**, and **C70⊂24** upon excitation at 575 nm; (c) **25**, **C60⊂25**, and **C70⊂25** upon excitation at 540 nm; and (d) the host-guest complex **C70⊂23** upon excitation at different pump wavelengths (575, 540 and 515 nm). (e) Spectral decomposition of transient absorption data for complex **C70⊂23** and (f) the corresponding population kinetics. Reproduced with permission [68]. Copyright 2017, American Chemical Society.

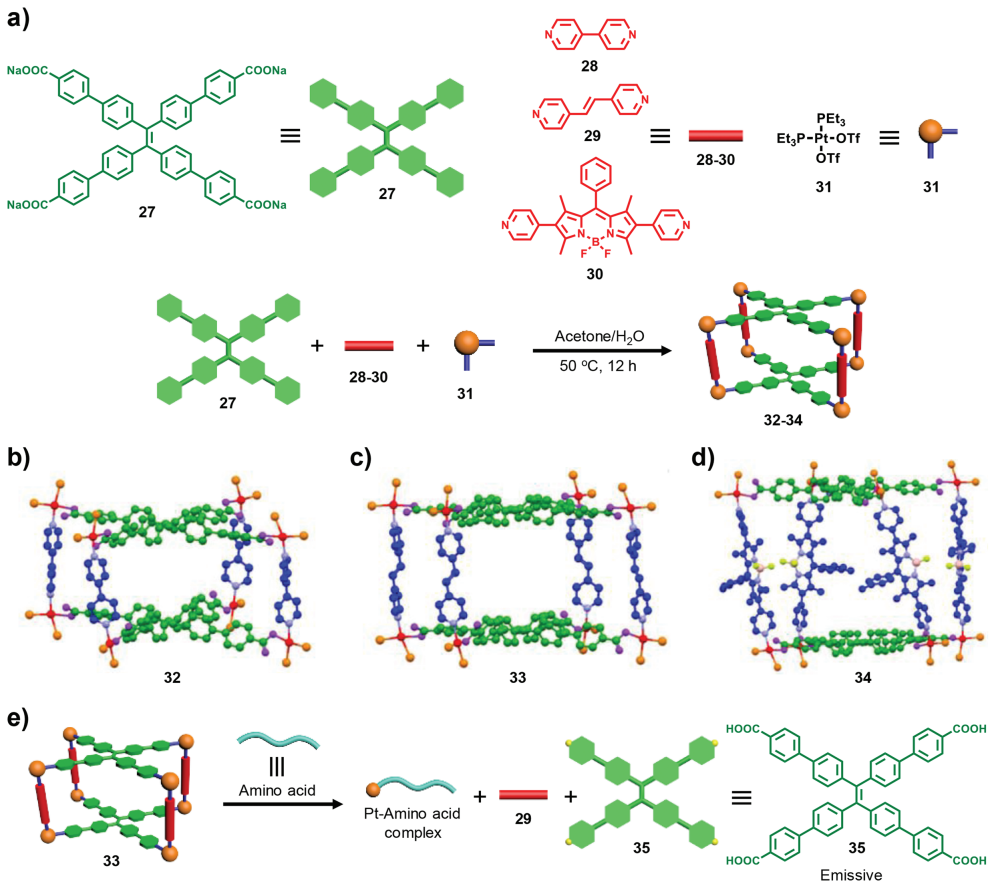


**Fig. 5.** (a) Self-assembly of carboxylate ligand **27**, dipyridyl ligands **28**-**30** and 90° Pt(II) acceptors **31** into cages **32**-**34**. (b-d) Simulated molecular structures of cages **32**-**34**. (e) Schematic representation mechanism for self-destruction of cage **33** in thiol-containing amino acid sensing. Reproduced with permission [71]. Copyright 2017, American Chemical Society.

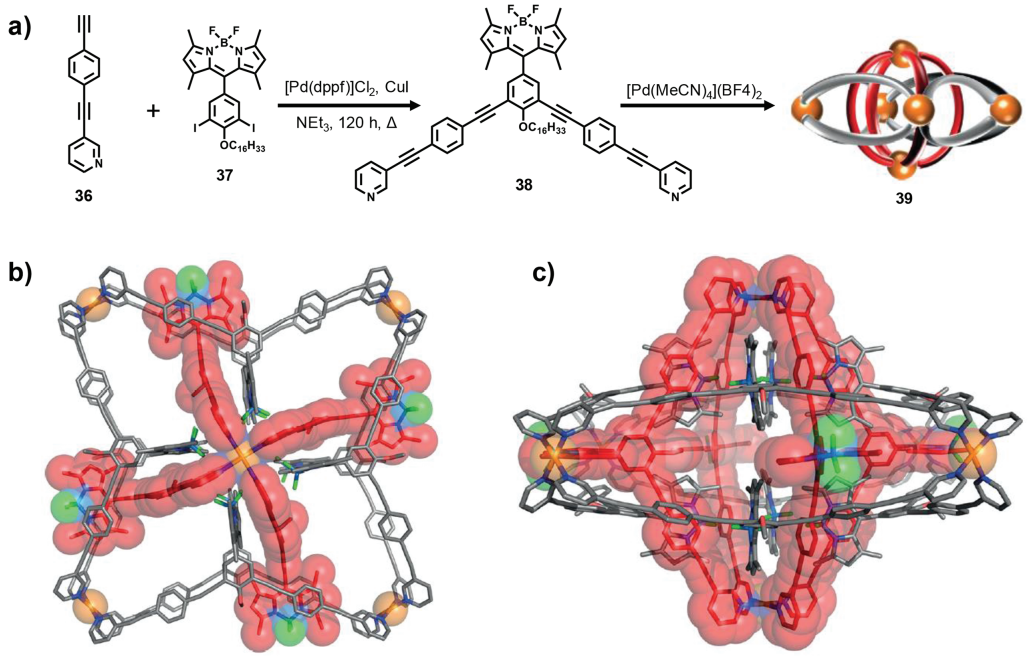


**Fig. 6.** (a) Synthesis of BODIPY-containing precursor **38** and subsequent self-assembly into rotaxane-like complex **39**. (b, c) X-ray crystal structure of complex **39** in two different orientations. Reproduced with permission [72]. Copyright 2018, Wiley Publishing Group.

peaks at 282 nm and 318 nm in $CH_2Cl_2$, respectively, and strong fluorescence at 493 nm, which was attributed to emission from TPE groups. For cage **34**, a sharp absorption band at 520 nm was observed in addition to the two broad absorptions at 278 and 319 nm, which were absorptions by BODIPY groups. The fluorescence of **34** also showed two peaks at 472 and 544 nm due to the presence of two different chromophores, TPE and BODIPY. In addition, the fluorescence quantum yields of **32**–**34** were 0.25, 0.2 and 0.13 in DMSO, respectively, suggesting that the dipyridyl ligands exerted a great influence on the photophysical properties of the cages through coordination-induced emission of TPE subunits. Moreover, the fluorescence quantum yields of the cages varied largely with the solvent (0.02 and 0.13 for **34** in $CH_2Cl_2$ and DMSO, respectively). Furthermore, the application of cage **33** as a "turn-on" sensor for amino acids was explored. Upon addition of thiol-containing amino acids such as glutathione and cysteine, the fluorescence intensity of **33** showed a remarkable increase at 500 nm and was almost proportional to the concentration of the amino acid (0−80 μmol/L). In addition, the detection limits were very low (0.189 and 0.278 μmol/L for glutathione and cysteine, respectively), and **33** showed no response to other amino acids, indicating that **33** may serve as a good fluorescent sensor for thiol-containing amino acids (Fig. 5e). The combined NMR and mass spectral results revealed the self-destructive mechanism of amino acid sensing, and the cage could be recovered upon addition of 90° Pt(II) acceptors, further confirming the stimuli-responsive properties of the multicomponent emissive cages.

As a result of the simple planar coordination mode for Pd as well as the developmental maturity of Pd-based SCCs, a variety of Pd-based SCCs, especially $M_nL_{2n}$-type supramolecules, have been constructed in the past few decades and have displayed wide-ranging applications in host-guest chemistry and catalysis. In 2018, Lützen and Käseborn *et al*. reported the synthesis of a rotaxane-like $Pd_6L_{12}$ metallosupramolecular architecture with structural complexity based on the BODIPY chromophore [72]. BODIPY-containing ligand **38** was readily prepared in four steps (Fig. 6a). By reacting ligand **38** with $[Pd(CH_3CN)_4](BF_4)_2$ in a molar ratio of 2:1 in acetonitrile-$d_3$/dichloromethane-$d_2$ (5:1), an unexpected feature was observed in its NMR spectrum in which the pyridine resonances were split into three sets of signals, suggesting structural complexity. Even though the ESI-MS spectrum indicated exclusive formation of a $Pd_6L_{12}$ supramolecular assembly, the combined $^1$H NMR, $^{19}$F NMR and 2D NMR results revealed that the complex obtained was not like previously reported $Pd_6L_{12}$ supramolecular architectures. Furthermore, a single crystal of the complex was grown in DMF/benzene, and X-ray diffraction results indicated that complex **39** adopted a rotaxane-like cage-in-ring arrangement (Figs. 6b and c). The giant complex consisted of two parts, a typical $Pd_2L_4$ cage with a Pd–Pd distance of 23.6 Å and a crown-like $Pd_4L_8$ macrocycle with neighbouring Pd–Pd distances of 27.9 and 28.0 Å. For the cage-like $Pd_2L_4$ part of the complex, the ligands exhibited a C-shaped conformation in which the BODIPY moieties and the long alkoxy chains were pointed outwards and inwards from the cage, respectively. In the macrocyclic $Pd_4L_8$ part of the complex, the ligands adopted a W-shaped conformation, and the BODIPY moieties and the long alkoxy chains were pointed inwards and outwards from the complex, respectively, completely unlike those in the $Pd_2L_4$ part. Therefore, a distinctive rotaxane-like complex **39** was formed, and the BODIPY-containing ligands in the complex were mechanically interpenetrated without being catenated. One ligand with a different conformation in one entity was uncommon in previously reported SCCs, and this arrangement led to significant $\pi$-stacking interactions between the BODIPY moieties and ligand skeletons, which further enhanced the stability of the complex. In addition, the NMR and MS experiments indicated extremely fast formation of the $Pd_6L_{12}$ complex (within 5–10 min), which also suggested the excellent stability of the complex. Furthermore, spectroscopic experiments were conducted, and the results revealed that the absorption spectra of the ligands showed negligible changes upon coordination, while the fluorescence was partially quenched. This research provided successful construction of a rotaxane-like $Pd_6L_{12}$ metallosupramolecular architecture with structural complexity resulting from $\pi$-stacking interactions between the BODIPY-containing ligands, offering the possibility of constructing more complex and sophisticated SCCs through weak interactions such as $\pi$-$\pi$ and van der Waals interactions.

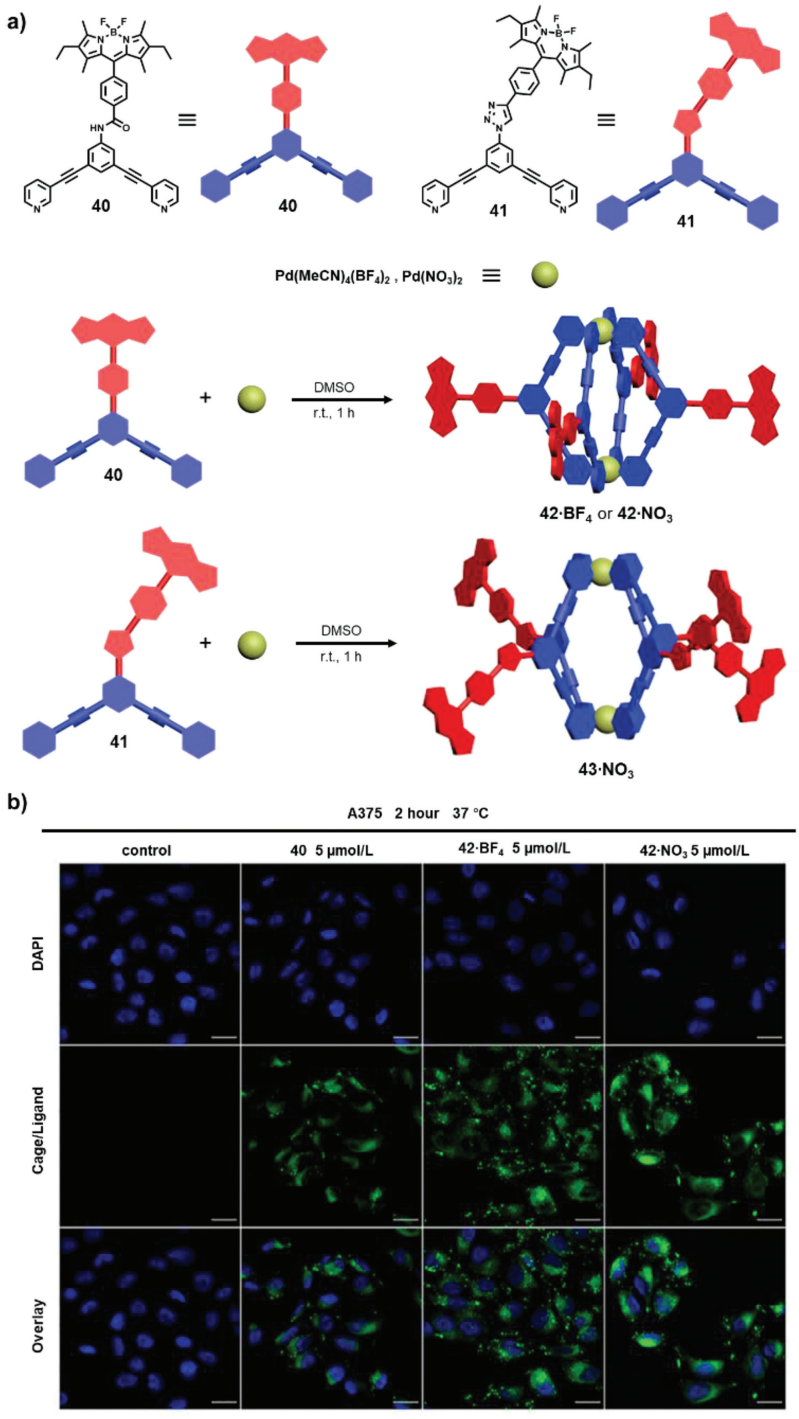


**Fig. 7.** (a) Synthesis of BODIPY-containing cages **42** and **43**. (b) Confocal laser scanning microscopy (CLSM) images of fixed human A375 melanoma cells upon treatment with ligand **40** or cages **42·BF$_4$** and **42·NO$_3$** for 2 h at 37 °C. Reproduced with permission [73]. Copyright 2019, Elsevier.

Construction of fluorescent SCCs with high fluorescence quantum yields is still challenging because of fluorescence quenching resulting from the "heavy-atom effect". In 2019, Casini and coworkers reported the construction of a series of highly emissive BODIPY-based supramolecular cages and investigated their utility in cell imaging [73]. Treatment of BODIPY-functionalized dipyridyl ligands **40** or **41** with $[Pd(CH_3CN)_4](BF_4)_2$ or $Pd(NO_3)_2$ in DMSO at room temperature afforded BODIPY-containing cages **42** and **43**, respectively (the counter anions were different due to the Pd precursors) (Fig. 7a). The cages were well characterized with NMR and mass spectrometry. Spectroscopic experiments indicated that the cages showed two main absorption bands at 290 and 520 nm with relatively high fluorescence quantum yields of 0.5–0.7. Notably, the amide and azido group linkers reduced the conjugation between the BODIPY chromophore and the Pd metal and enabled efficient emission from the cages. Furthermore, the stabilities of the cages in biological systems were studied, and the results from UV–visible absorption spectra showed that all cages were completely stable in water, whereas **42·BF$_4$** and **42·NO$_3$** showed moderate stability for 24 h in PBS buffer. However, the absorption intensity for cage **43·NO$_3$** showed a large decrease in PBS buffer, suggesting instability resulting from poor solubility in physiological media. In addi-

tion, NMR titration results indicated that **42·$BF_4$** and **42·$NO_3$** disassembled into ligands upon addition of physiologically relevant concentrations of glutathione. Moreover, the slight downfield shifts of $^1$H NMR signals corresponding to the pyridines and the upfield shifts for $^{195}$Pt NMR signals upon addition of cisplatin both proved efficient encapsulation of 2 equiv. of cisplatin into the cages **42·$BF_4$** and **42·$NO_3$**. Furthermore, the antiproliferative effects of the cages were studied (Fig. 7b), and cage **42** showed no toxicity against human A375 cells and an EC50 of more than 50 mmol/L; however, host-guest complexes of the cages with cisplatin exhibited antiproliferative effects similar to those of cisplatin. Using the highly emissive character of the BODIPY-containing cages, uptake and cellular localization studies of the cages were conducted with confocal fluorescence microscopy imaging. The results indicated that the **42·$BF_4$** and **42·$NO_3$** cages mainly accumulated in intracellular vesicles. In addition, the cells showed no uptake of the cages at low temperature (4 °C), demonstrating that energy-independent endocytic transport was the main pathway for cell uptake.

## 3. Conclusion

During recent decades, BODIPY-based supramolecular cages with distinctive properties and functions have been successfully constructed, and they have displayed various intriguing applications. For example, due to the high fluorescence quantum yields and efficient singlet oxygen generation by BODIPY chromophores, BODIPY-based cages exhibited bright emission and $^1O_2$ generation, which could be applied in fluorescent sensors, single-component white emission and photodriven autocatalysis. In addition, the cages with well-defined shapes and sizes enabled efficient excitation energy delocalization by the BODIPY chromophores and subsequent charge transfer to the guests. Moreover, BODIPY chromophores with relatively planar conformations exhibited significant $\pi$-$\pi$ stacking interactions with other subunits, offering the possibility of constructing new SCCs with greater structural complexity. It should be noted that when the BODIPY fluorophore was directly used as the backbone, the BODIPY-based metallacages usually display different photophysical/chemical properties, including fluorescence and photosensitization properties, to the ligands as well as the typical BODIPY fluorophores and largely lied on the cage structure. While when the BODIPY fluorophore was attached to the peripheries of cages, the BODIPY-based metallacages usually maintain the photophysical/chemical properties as the BODIPY-based ligands. In a word, the BODIPY-based metallacages inherently inherit the high molar absorption coefficient and excellent fluorescence and photosensitization property of the BODIPY fluorophore and exhibited multi-fluorophore interactions within the cages, which was beneficial for the construction of artificial light-harvesting systems and photocatalysis. However, due to the planar structure of the BODIPY fluorophore, the metallacages usually showed low fluorescence in the aggregate state, which hampered their applications in solid-state emissive materials, even though some AIE-active metallacages showed superiority in this filed.

Although some achievements have been realized in syntheses and property investigations of BODIPY-based cages, this area is still in its infancy, and more in-depth investigations are needed. To name a few, the host-guest chemistry of BODIPY-containing cages has been studied insufficiently, and the guests are limited to fullerene. Second, even though BODIPY is a typical photosensitizer for photodynamic therapy (PDT), there have been no investigations of phototherapeutic applications of BODIPY-based cages to date. Therefore, some improvements should be considered while further developing BODIPY-based supramolecular cages. On the one hand, the structural diversity of the cages should be developed to bind more kinds of guests and further promote their use in molecular sensing, catalysis and light-harvesting. For instance, geometrical configurations of the cages, such as Platonic and Archimedes polyhedra, the metal vertexes and the molecular structures of the BODIPY-containing ligands should be designed judiciously to induce high affinity for targeted guests. Furthermore, the well-aligned chormophore within the BODIPY-containing cages could be explored in the construction of artificial photosynthesis systems. On the other hand, in order to investigate biological applications of BODIPY-based cages, construction of water-soluble BODIPY-containing cages will enhance their biocompatibility. In conclusion, BODIPY-based cages might give rise to increasing attention, and more widespread applications of BODIPY-containing cages in supramolecular chemistry and materials science will be predicted in the future.

## Declaration of competing interest

The authors declare that they have no known competing financial interests or personal relationships that could have appeared to influence the work reported in this paper.

## Acknowledgments

This work was supported by the Program of Shanghai Outstanding Academic Leaders (No. 21XD1421200) and the Fundamental Research Funds for the Central Universities. Y. Qin acknowledges the financial support sponsored by the National Natural Science Foundation of China (No. 22101183) and China Postdoctoral Science Foundation (No. 2021M702251).

## References

[1] M. Fujita, M. Tominaga, A. Hori, B. Therrien, Acc. Chem. Res. 38 (2005) 369–378.
[2] R. Chakrabarty, P.S. Mukherjee, P.J. Stang, Chem. Rev. 111 (2011) 6810–6918.
[3] W.X. Gao, H.N. Zhang, G.X. Jin, Coord. Chem. Rev. 386 (2019) 69–84.
[4] H. Ube, K. Endo, H. Sato, M. Shionoya, J. Am. Chem. Soc. 141 (2019) 10384–10389.
[5] J.L. Zhu, D. Zhang, T.K. Ronson, et al., Angew. Chem. Int. Ed. 60 (2021) 11789–11792.
[6] X. Yan, T.R. Cook, P. Wang, F. Huang, P.J. Stang, Nat. Chem. 7 (2015) 342–348.
[7] M. Yoshizawa, L. Catti, Acc. Chem. Res. 52 (2019) 2392–2404.
[8] D. Luo, X.Z. Wang, C. Yang, X.P. Zhou, D. Li, J. Am. Chem. Soc. 140 (2018) 118–121.
[9] R.J. Li, J.J. Holstein, W.G. Hiller, J. Andréasson, G.H. Clever, J. Am. Chem. Soc. 141 (2019) 2097–2103.
[10] T. Kim, N. Singh, J. Oh, et al., J. Am. Chem. Soc. 138 (2016) 8368–8371.
[11] Y. Wang, Q. Zhou, X. He, et al., Chin. Chem. Lett. 33 (2022) 1613–1618.
[12] X.Z. Li, L.P. Zhou, L.L. Yan, et al., J. Am. Chem. Soc. 139 (2017) 8237–8244.
[13] L. Catti, H. Narita, Y. Tanaka, et al., J. Am. Chem. Soc. 143 (2021) 9361–9367.
[14] W. Cullen, M.C. Misuraca, C.A. Hunter, N.H. Williams, M.D. Ward, Nat. Chem. 8 (2016) 231–236.
[15] K. Li, K. Wu, Y.L. Lu, et al., Angew. Chem. Int. Ed. 61 (2022) e202114070.
[16] X. Gao, Z. Cui, Y.R. Shen, et al., J. Am. Chem. Soc. 143 (2021) 17833–17842.
[17] Q. Ling, T. Cheng, S. Tan, J. Huang, L. Xu, Chin. Chem. Lett. 31 (2020) 2884–2890.
[18] G. Li, Z. Zhou, C. Yuan, et al., Angew. Chem. Int. Ed. 59 (2020) 10013–10017.
[19] P.P. Jia, L. Xu, Y.X. Hu, et al., J. Am. Chem. Soc. 143 (2021) 399–408.
[20] M. Yamashina, Y. Tanaka, R. Lavendomme, et al., Nature 574 (2019) 511–515.
[21] S. Hasegawa, S.L. Meichsner, J.J. Holstein, et al., J. Am. Chem. Soc. 143 (2021) 9718–9723.
[22] Y.X. Hu, P.P. Jia, C.W. Zhang, et al., Org. Chem. Front. 8 (2021) 5250–5257.
[23] P. Howlader, S. Mondal, S. Ahmed, P.S. Mukherjee, J. Am. Chem. Soc. 142 (2020) 20968–20972.
[24] J.L. Zhu, L. Xu, Y.Y. Ren, et al., Nat. Commun. 10 (2019) 4285.
[25] H. Duan, Y. Li, Q. Li, et al., Angew. Chem. Int. Ed. 59 (2020) 10101–10110.
[26] X. Liu, Y. Qin, J. Zhu, et al., Chin. Chem. Lett. 32 (2021) 1537–1540.
[27] H.K. Li, H.L. Ye, X.X. Zhao, et al., Chin. Chem. Lett. 32 (2021) 2851–2855.
[28] E.G. Percástegui, T.K. Ronson, J.R. Nitschke, Chem. Rev. 120 (2020) 13480–13544.
[29] S. Pullen, G.H. Clever, Acc. Chem. Res. 51 (2018) 3052–3064.
[30] M. Pan, K. Wu, J.H. Zhang, C.Y. Su, Coord. Chem. Rev. 378 (2019) 333–349.
[31] M.D. Ward, C.A. Hunter, N.H. Williams, Acc. Chem. Res. 51 (2018) 2073–2082.
[32] X. Li, J. Zheng, W. Liu, et al., Chin. Chem. Lett. 31 (2020) 2937–2940.
[33] C.M. Hong, R.G. Bergman, K.N. Raymond, F.D. Toste, Acc. Chem. Res. 51 (2018) 2447–2455.
[34] H. Chen, W. Chen, Y. Lin, et al., Chin. Chem. Lett. 32 (2021) 2359–2368.
[35] Y.X. Hu, X. Hao, L. Xu, et al., J. Am. Chem. Soc. 142 (2020) 6285–6294.

[36] Q. Qi, S. Jiang, Q. Qiao, et al., Chin. Chem. Lett. 31 (2020) 2985–2987.
[37] Z. Zhang, Z. Zhao, L. Wu, et al., J. Am. Chem. Soc. 142 (2020) 2592–2600.
[38] M.L. Saha, X. Yan, P.J. Stang, Acc. Chem. Res. 49 (2016) 2527–2539.
[39] X. Jing, C. He, L. Zhao, C. Duan, Acc. Chem. Res. 52 (2019) 100–109.
[40] T. Liang, P. Yang, T. Wu, et al., Chin. Chem. Lett. 31 (2020) 2975–2979.
[41] C. Mu, Z. Zhang, Y. Hou, et al., Angew. Chem. Int. Ed. 60 (2021) 12293–12297.
[42] C. Yan, L. Shi, Z. Guo, W. Zhu, Chin. Chem. Lett. 30 (2019) 1849–1855.
[43] H. Zhu, Q. Li, B. Shi, et al., Angew. Chem. Int. Ed. 59 (2020) 20208–20214.
[44] W. Zhou, X. Fang, Q. Qiao, et al., Chin. Chem. Lett. 32 (2021) 943–946.
[45] J. Zhao, Z. Zhou, P.J. Stang, X. Yan, Natl. Sci. Rev. 8 (2021) nwab045.
[46] C. Li, B. Zhang, Y. Dong, et al., Dalton Trans. 49 (2020) 8051–8055.
[47] L. Xu, Y.X. Wang, H.B. Yang, Dalton Trans. 44 (2015) 867–890.
[48] H.Y. Lin, L.Y. Zhou, L. Xu, Chem. Asian J. 16 (2021) 3805–3816.
[49] H. Lu, J. Mack, Y. Yang, Z. Shen, Chem. Soc. Rev. 43 (2014) 4778–4823.
[50] A.N. Bismillah, I. Aprahamian, Chem. Soc. Rev. 50 (2021) 5631–5649.
[51] Z. Shi, X. Han, W. Hu, et al., Chem. Soc. Rev. 49 (2020) 7533–7567.
[52] X.X. Chen, L.Y. Niu, N. Shao, Q.Z. Yang, Anal. Chem. 91 (2019) 4301–4306.
[53] M.Q. Wang, J.J. Gao, Q.Q. Yu, H.B. Liu, New J. Chem. 44 (2020) 13557–13564.
[54] G. Gupta, Y. Sun, A. Das, P.J. Stang, C.Y. Lee, Coord. Chem. Rev. 452 (2022) 214308.
[55] S. Cherumukkil, G. Das, R.P.N. Tripathi, et al., Adv. Funct. Mater. 32 (2022) 2109041.
[56] F.Z. Li, J.F. Yin, G.C. Kuang, Coord. Chem. Rev. 448 (2021) 214157.
[57] P. Chinapang, H. Iwami, T. Enomoto, et al., Inorg. Chem. 60 (2021) 12634–12643.
[58] J. Zhou, Y. Zhang, G. Yu, et al., J. Am. Chem. Soc. 140 (2018) 7730–7736.
[59] C. Li, P.P. Jia, Y.L. Xu, et al., Sci. China Chem. 64 (2021) 134–142.
[60] G. Li, X. Zhang, W. Zhao, et al., ACS Appl. Mater. Interfaces 12 (2020) 20180–20190.
[61] Y. Qin, X. Liu, P.P. Jia, L. Xu, H.B. Yang, Chem. Soc. Rev. 49 (2020) 5678–5703.
[62] D. Zhang, T.K. Ronson, J.R. Nitschke, Acc. Chem. Res. 51 (2018) 2423–2436.
[63] P.P. Neelakandan, A. Jiménez, J.R. Nitschke, Chem. Sci. 5 (2014) 908–915.
[64] L.K.S. von Krbek, D.A. Roberts, B.S. Pilgrim, C.A. Schalley, J.R. Nitschke, Angew. Chem. Int. Ed. 57 (2018) 14121–14124.
[65] P.P. Neelakandan, J.D.T A.Jiménez, J.R. Nitschke, Angew. Chem. Int. Ed. 54 (2015) 14378–14382.
[66] Y.R. Hristova, M.M.J. Smulders, J.K. Clegg, B. Breiner, J.R. Nitschke, Chem. Sci. 2 (2011) 638–641.
[67] C. Hansch, A. Leo, R.W. Taft, Chem. Rev. 91 (1991) 165.
[68] A.J. Musser, P.P. Neelakandan, J.M. Richter, et al., J. Am. Chem. Soc. 139 (2017) 12050–12059.
[69] P.D. Frischmann, V. Kunz, F. Würthner, Angew. Chem. Int. Ed. 54 (2015) 7285–7289.
[70] P.D. Frischmann, V. Kunz, V. Stepanenko, F. Würthner, Chem. Eur. J. 21 (2015) 2766–2769.
[71] M. Zhang, M.L. Saha, M. Wang, et al., J. Am. Chem. Soc. 139 (2017) 5067–5074.
[72] M. Käseborn, J.J. Holstein, G.H. Clever, A. Lützen, Angew. Chem. Int. Ed. 57 (2018) 12171–12175.
[73] B. Woods, D. Döllerer, B. Aikman, et al., J. Inorg. Biochem. 199 (2019) 110781.